On formation of a shock wave in front of a coronal mass ejection with velocity exceeding the critical one

M. V. Eselevich[1] and V. G. Eselevich[1]

Received 25 July 2008; accepted 20 October 2008; published 22 November 2008.

[1] It is shown that in front of a coronal mass ejection, having a velocity u lower than the critical u_C relative to the surrounding coronal plasma, there is a disturbed region expended along a direction of the CME propagation. The time difference brightness (plasma density) in the disturbed region smoothly decreases to larger distances in front of the CME. A discontinuity forms at u higher than u_C in the disturbed region front part in radial distributions of the difference brightness. Since the u_C value is close to the local fast-mode MHD velocity, which in corona approximately equal to the Alfven one, the formation of such a discontinuity when u_C is exceeded may be identified with the formation of a shock wave. **Citation:** Eselevich, M. V., and V. G. Eselevich (2008), On formation of a shock wave in front of a coronal mass ejection with velocity exceeding the critical one, *Geophys. Res. Lett.*, *35*, L22105, doi:10.1029/2008GL035482.

1. Introduction

[2] A coronal mass ejection (CME) structure in white light is often characterized by the following well-known features: a bright frontal structure (FS) that covers the region of decreased plasma density (cavity) that may includes a bright interior (core). However, besides the said features, another extended disturbed region defined by *Eselevich and Eselevich* [2007] can exist immediately in front of a CME. The aim of our study is to investigate changes in the disturbed region form, when a CME velocity increases, and possibilities for formation of a shock wave in this case.

2. Method of Analysis

[3] In the analysis, corona images obtained with the LASCO-C2 and C3/SOHO [*Brueckner et al.*, 1995] were represented as the difference brightness $\Delta P = P(t) - P(t_0)$, where $P(t_0)$ is the undisturbed brightness at t_0 before the event considered, $P(t)$ is the disturbed brightness at any instant $t > t_0$. Calibrated LASCO images were employed with the total brightness $P(t)$ expressed in units of the mean solar brightness (P_{msb}).

[4] The excess mass ρ (in g cm^{-2}) (a quantitative characteristic that corresponds to change in mass of the plasma column, orientated along the line of sight and having the unit area of the base) was calculated from the difference brightness ΔP. By analogy with *Jackson and Hildner* [1978], all plasma in the column was assumed to be in the plane of the sky. To represent difference white-corona images as an excess mass appears convenient, because this value includes the radial filter, compensating brightness rapid decrease with distance in the corona, and also allows estimation of CME mass. Distribution profiles $\Delta P(R)$ and $\rho(R)$ are almost identical on a scale in the order of the solar radius.

[5] Images of the excess mass were employed to investigate the CME dynamics and disturbed region. For the purpose we used presentations in the form of isolines and sections both along the solar radius at fixed position angles PA and non-radial sections at various instants t. On all the images, the position angle PA was counted counterclockwise from the Sun's north pole.

3. Data Analysis

[6] The CMEs are investigated that appear at ~40 degrees of longitude relative to the plane of the limb. It means that their velocity V, measured in a projection on the plane of the sky, does not considerably exceed the true radial CME velocity.

[7] First we consider two CMEs (CME1 and CME2) whose velocities V differ greatly at $R = (4–5)\ R_\odot$ ($R_\odot$ is the solar radius). Figures 1a and 1c show the typical excess-mass form (in isolines) for these two CMEs at the instants, when their frontal structures FS appear in the C2 field of view. Figure 1a presents the slow CME1 (7 May 1997, $t - t_0$ = 12:29–04:51; $V \approx 230$ km s^{-1}), Figure 1c the fast CME2 (25 July 1999, $t - t_0$ = 13:52–12:28; $V \approx 1390$ km s^{-1}). The velocity V values corresponding to the fastest front parts of the CMEs have been taken from the CME catalogue (http://cdaw.gsfc.nasa.gov/CME_list/). Figures 1a and 1c show that on the images of both CMEs the frontal structure FS can approximately be presented by a part of a circle with its center at O (dots on Figure 1). The radius of circle r and its center O were selected such that the circle coincided best with the position of FS maxima.

[8] The main direction of the CME propagation that roughly coincides with its symmetry axis is indicated by a heavy dashed line a. This line was drawn through the Sun center and the center of the CME, O. It passes along the streamer belt or streamer chains [*Eselevich et al.*, 1999, 2007]; i.e., it is in the region of the quasistationary slow solar wind (SW).

[9] In order to find the left boundary of the disturbed region (from the CME side), by analogy with *Mouschovias and Poland* [1978] we determine the FS width h as a width at a half-height of the excess mass $\rho(r)$ distribution constructed from the CME center. For CME1, the frontal structure in the direction of section b (Figure 1a) is least distorted by the disturbed region effect and has a minimum width $h \approx 0.3\ R_\odot$ (a curve with black circles in Figure 1b).

[1]Institute of Solar-Terrestrial Physics, Irkutsk, Russia.

0094-8276/08/2008GL035482$05.00

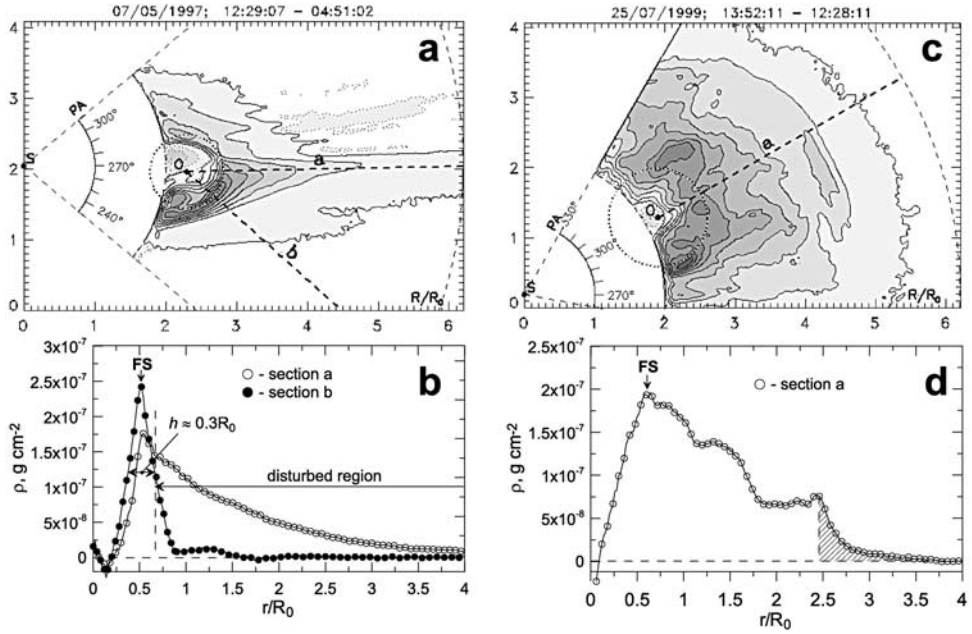

Figure 1. (a and b) Slow CME on 1997 May 7 (CME1 in the text, $V \approx 230$ km s^{-1}); (c and d) fast on 1999 July 25 (CME2 in the text, $V \approx 1390$ km s^{-1}); Figures 1a and 1c display images of the excess mass in the form of isolines; *PA* is the position angle; Figures 1b and 1d present distributions of the excess mass depending on the distance *r*, calculated from the CME center (point O) along two different sections a and b, whose directions are shown on Figures 1a and 1c.

This value correlates within the limits of error with the mean along the FS, typical value h at $R \approx 2.8\ R_\odot$ from the Sun center found for several CMEs in the work of *Mouschovias and Poland* [1978].

[10] Take the right FS boundary as the left one of the disturbed region as is shown in Figure 1b. Its position is indicated by a vertical dashed line. In Figure 1b, a curve with light circles shows the $\rho(r)$ distribution along the section a in the direction of the CME propagation. The disturbed region is marked by a horizontal line with arrow and inscription "disturbed region".

[11] The comparison between CME1 (slow) and CME2 (fast) yields two principal distinctions:

[12] 1. The isolines that correspond to the minimum excess mass of the slow CME1 are extended along the direction of its propagation, while those of the fast one are close in form to a circle.

[13] 2. The excess mass $\rho(R)$ distribution along the direction of the CME propagation continuously decreases up to the most remote front part of the disturbed region for the slow CME, whereas in the front part of the fast CME disturbed region a discontinuity appears in the $\rho(R)$ distribution on a typical scale $\delta_F \approx 0.3\ R_\odot$ (hatched in Figure 1d).

[14] The $\rho(R)$ distributions constructed along the direction of the CME propagation are presented for the set of nine CMEs in Figure 2. CME velocities are different and increase from bottom to top in Figure 2, thus the slowest CME with $V \approx 370$ km s^{-1} is shown in Figure 2 (bottom), and the fastest one with $V \approx 2400$ km s^{-1} Figure 2 (top). Light circles indicate undisturbed distributions of $\rho(R)$ corresponding to the instants before the CMEs appear. These distributions can serve as estimation for a random noise level at different distances. Figure 2 implies that at CME velocities V higher than a critical velocity V_C there is a discontinuity in $\rho(R)$ distributions at the front boundary of the disturbed region (hatched parts). At the same time at $V < V_C$ such discontinuity is absent, and the excess mass distribution smoothly decreases with increasing distance until it becomes indistinguishable on a noise level.

[15] The CMEs considered did not actually occur exactly at the limb; hence their radial velocity may be somewhat higher than the values in Figure 2. This implies that for a CME with discontinuity (with $V \approx 900$ km s^{-1} and higher) the condition that its velocity exceed V_C works more reliably. The CME on 23 February 1997, whose velocity ($V \approx 900$ km s^{-1}) appears to be the closest (from above) to the critical value V_C, propagated virtually in the plane of the sky, since the longitude of its source was offset from the E limb only by $\approx 8 \pm 4$ degrees according to *Cremades and Bothmer* [2004, Table 1]. Discontinuity-free CMEs with below-V_C velocities may cause some doubts. The longitude at which the 1998 June 2 CME ($V \approx 750$ km s^{-1}) was born was offset from the W limb by $\approx 19 \pm 17$ degrees [*Cremades and Bothmer*, 2004, Table 1]. The CMEs on 29 September and 23 April 1997 are associated with the limb eruptive prominences, which occurred respectively on 29 September 1997, at 12:54 UT (*PA* = 68 degrees) (SGD, http://sgd.ngdc.noaa.gov/sgd/jsp/solarindex.jsp) and on 23 April 1997, at 03:01 UT (*PA* = 66 degrees) (Nobeyama, http://solar.nro.nao.ac.jp/). Therefore, they must all propagate practically in the plane of the sky, with their radial velocity differing only slightly from the observed velocity. The last CME of 8 May 1998 had a rather low velocity ($V \approx$

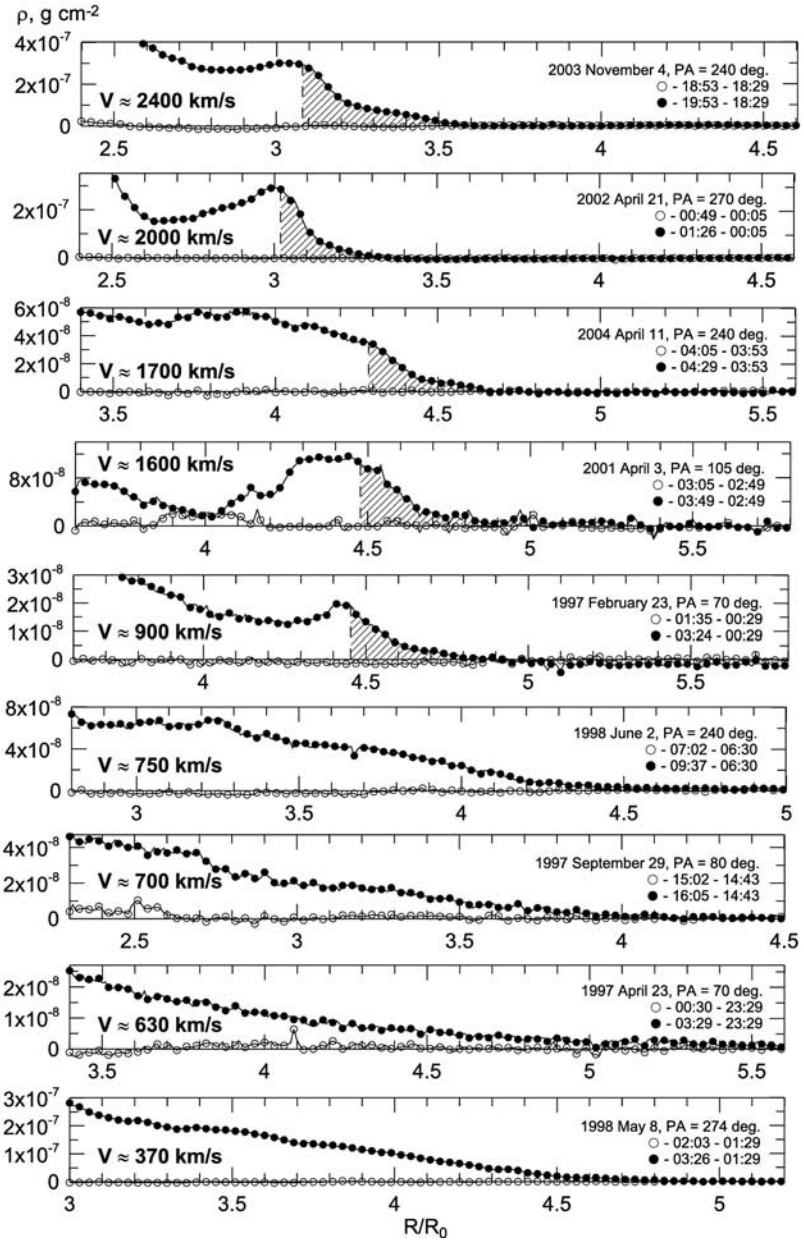

Figure 2. The $\rho(R)$ distributions for 9 CMEs (black circles) along the direction of their propagation. The CME velocities increase from the bottom plot to the top plot. Light circles show the undisturbed distributions of $\rho(R)$ before the CMEs appeared.

370 km s^{-1}), therefore its radial velocity was always less than V_C.

[16] Obviously, in processes of the "CME – undisturbed coronal plasma" interaction a crucial role should play not simply a V value, but a value of CME velocity relative to the surrounding SW stream $u = V - V_{SW}$. Since CME velocities were determined in the direction of their propagation, we took a velocity of the slow SW flowing for the most part in the region of the coronal streamer belt and streamer chains, along which the majority of CMEs move, as the velocity V_{SW} of the undisturbed solar wind [*Hundhausen*, 1993; *Eselevich*, 1995].

[17] Figure 3 presents values of the relative velocity u measured for eighteen different CMEs at different distances. For $V_{SW}(R)$ we employed dependence derived by *Wang et al.* [2000] of the slow SW velocity on the distance R in the streamer belt. This dependence is shown by a dash-dot line in Figure 3.

[18] In Figure 3, solid marks correspond to the CMEs having a discontinuity in the difference brightness distributions in front of the disturbed region. CME velocities V were determined from the discontinuity motion. Light marks in Figure 3 indicate the CME without discontinuity. In this case we took a velocity from the CME catalogue. Figure 3 shows that the cases with the discontinuity observed are in the high-velocity region, and the cases without discontinuity (the disturbed region smoothly decreased with distance is observed there) are for the most part in the low-velocity region. Hence we can assume that the discontinuity forms, when the relative CME velocity u exceeds some

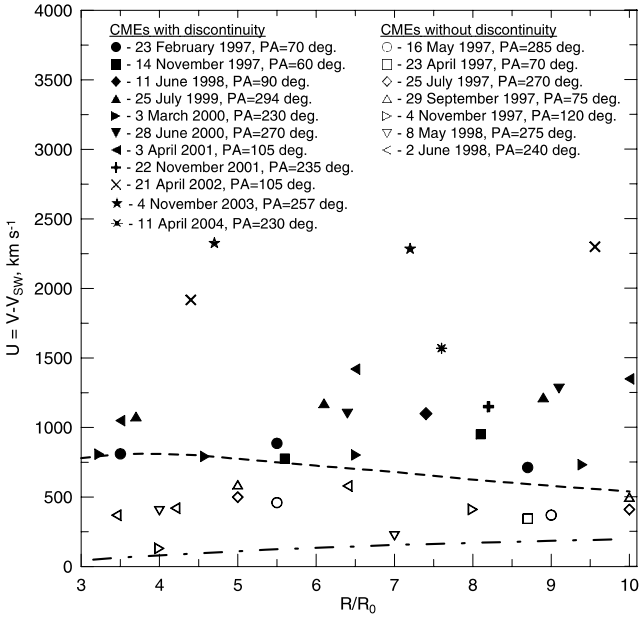

Figure 3. CME velocities $u = V - V_{SW}$ relative to the surrounding SW depending on a distance from the solar center for the CME without discontinuity (light marks) and the CME with discontinuity (dark marks). The dash-dot curve indicates the velocity V_{SW} of the quasistationary slow SW in the streamer belt from *Wang et al.* [2000]. The dash curve shows the Alfven velocity in the streamer belt from *Mann et al.* [1999].

critical u_C value. A critical velocity value may depend on a distance R.

[19] Compare the obtained u_C value with the typical velocity of disturbance propagation in the magnetized corona plasma that roughly equal to the velocity of magnetoacoustic waves in the plasma $V_{MS} \approx (V_S^2 + V_A^2)^{1/2}$. Here $V_S \approx (\gamma 2kT/m_p)^{1/2}$ is the sound velocity ($T_p \approx T_e = T$, k – Boltzmann constant, γ – adiabatic index) and $V_A = B/(4\pi N m_p)^{1/2}$ is the Alfven velocity (B – magnetic field, N – plasma density, m_p – proton mass). For the corona temperature $T \sim 10^6$K, the value $V_S \sim$ 150 km s^{-1}, whereas the Alfven velocity at $R \approx (2–10)$ $R_\odot$ presumably exceeds 500 km s^{-1}. Thus in order to estimate V_{MS} at these distances we may use V_A assuming that $V_{MS} \approx V_A$. In Figure 3, a dash line indicates the $V_A(R)$ dependence obtained by *Mann et al.* [1999].

[20] Obviously in Figure 3 the Alfven velocity passes approximately between clusters of points, which apply to the CMEs with discontinuity and without it. Hence $u_C \sim V_A$, i.e., the desired critical velocity is roughly equal to the typical velocity of disturbance propagation in the magnetized plasma.

[21] An analogy with gas flow around a body in gas dynamics can be drawn. Choose a CME-associated coordinate system, where an undisturbed SW stream flows around the CME at u. Given $u < V_A$, the disturbances appearing due to interaction between SW stream and CME and having the typical velocity close to V_A can go upstream as far as possible. This leads to a disturbed region formation. If the relative velocity $u > V_A$, disturbances can not outrun the stream and, being accumulated near the CME, make up a shock-wave discontinuity apparent in $\rho(R)$ distributions. A characteristic scale of the discontinuity δ_F should be determined by the energy dissipation mechanism in the discontinuity. Hence we have a situation the classical gasdynamics refers to as "transonic transition" and formation of a shock wave. It was predicted theoretically, but it is first observed experimentally in the magnetized plasma.

[22] Note that the presence of a shock wave in front of a CME is supported by other experiments. During shock front passage: in the 1998 June 11 event, the emission of the O VI and Si XII lines intensified according to SOHO/UVCS spectrum [*Raymond et al.*, 2000]; in the 2000 March 3 event, the spectral profiles of both the O VI and Lyα lines were Doppler dimmed and broadened [*Mancuso et al.*, 2002]; in the 2000 June 28 event, the O VI profile was broadened [*Ciaravella et al.*, 2005].

4. On possibility for Resolution of a Shock Front Width

[23] The problem of a possibility for resolution of a shock front width in the corona was considered in detail by *Eselevich and Eselevich* [2008]. Here we will briefly mention it. The discontinuity is observed in distributions of the excess mass $\rho(R)$ (or the difference brightness $\Delta P(R)$ equivalent to it) that results from free-electron scattering and is averaged along the line of sight in the optically thin corona. Since we do not know exactly the matter-density distribution along the line of sight, the observable scale δ_F in $\Delta P(R)$ distributions may differ from a real scale δ_N of the plasma density discontinuity. As a result of the averaging the observable discontinuity in the difference brightness profile can have larger scale than the real discontinuity in the density profile has.

[24] In order to estimate an effect of such averaging, δ_F/δ_N ratios were found in the context of a simple geometrical shock-front model in the work of *Eselevich and Eselevich* [2008]. Since on corona images the shock front has a form close to a circle part (see Figure 1c), we can assume that the front form is the same along the line of sight; i.e., it close to a sphere part at least in the direction of CME propagation. In the model considered, the shock-wave front was represented as a spherical shell with an outer radius R_F; the center of the shell was in the plane of the sky at R_C from the solar center (these parameters were specified according to the CME form). The brightness distribution $P(R)$, induced by free-electron scattering within the shell in the range from the shell center to its front edge, was calculated. At the given distance R, the brightness value is defined by the integral along the line of sight (in the l direction):

$$P(R) = \int_l i(R,\theta) N(R) dl \qquad (1)$$

where $i(R, \theta)$ is the brightness induced by the one-electron scattering, $N(r)$ – density. The $i(R, \theta)$ function depends on a distance R and an angle θ relative to the plane of the sky. The function values were calculated with the ELTHEORY procedure from SolarSoft in which formulas from *Billings* [1966] had been realized. In the spherical shell, the density

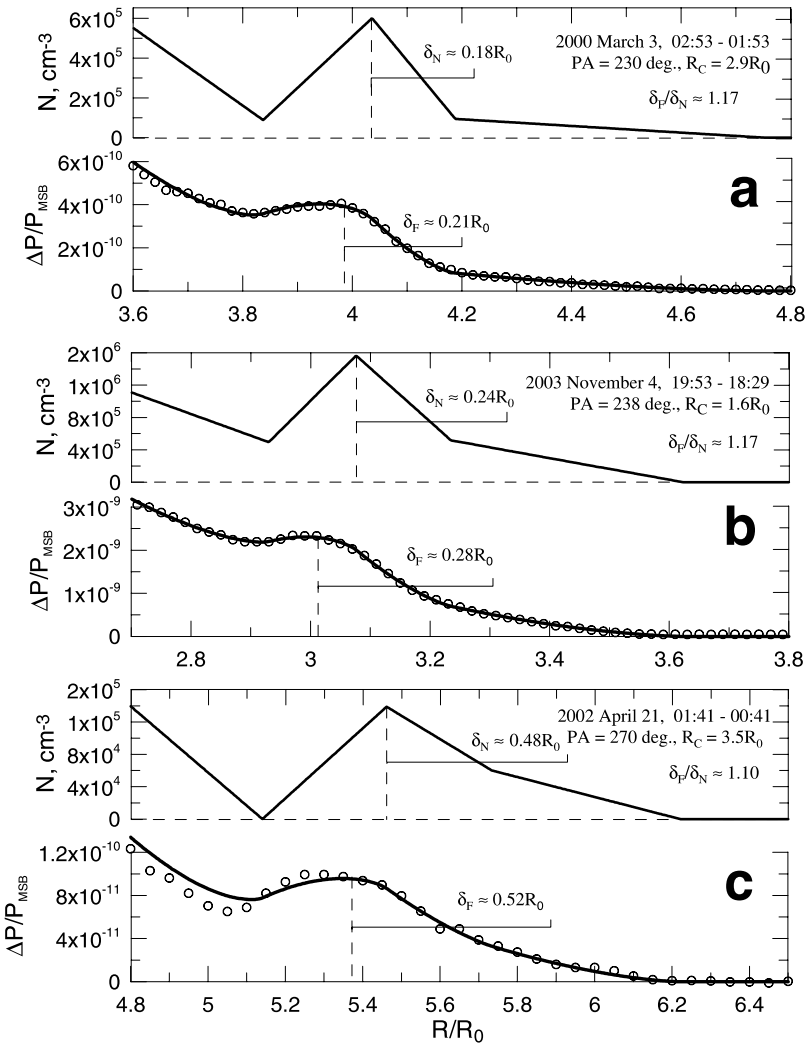

Figure 4. (a–c) Examples of calculation of the brightness profile in the context of the spherical shell model and comparison with experimental brightness profiles for three CMEs. Density profiles calculated (Figures 4a (top), 4b (top), and 4c (top)); difference brightness experimental profiles (light circles) and the calculated brightness profiles (solid lines) (Figures 4a (bottom), 4b (bottom), and 4c (bottom)). Scales of discontinuities are shown to be δ_F and δ_N respectively for each brightness and density profiles.

was supposed to change only depending on the distance r from the sphere center. In each case we chose a density profile $N(r)$ such that a model brightness profile $P(R)$ obtained from $N(r)$ by integration of equation (2) showed the best correlation with the experimental profile of the difference brightness $\Delta P(R)$. Then a scale δ_N of the plasma density discontinuity was found from the density profile $N(r)$ obtained.

[25] Figure 4 demonstrates three examples that present the calculation results. Obviously broadening of the $\Delta P(R)$ profile in comparison with the density profile $N(r)$ does not exceed 20%. The said examples correspond to different CMEs, angular sizes of which are from 60 to 120 degrees and which are registered at distances from 4 $R_\odot$ to 6 $R_\odot$ from the solar center.

[26] The analysis of many events confirms that the δ_F/δ_N value depends neither on a CME angular size nor on a distance from the Sun, where a shock front is registered. Thus, scale of a brightness profile discontinuity is a good approximation for determining scale of a density discontinuity in a shock wave front.

[27] **Conclusions** It has been shown that in front of a coronal mass ejection having a velocity u lower than the critical u_C relative to the surrounding coronal plasma there is a disturbed region expended along a direction of the CME propagation. The time difference brightness ΔP in the disturbed region smoothly decreases up to larger distances in front of the CME. Given $u > u_C$, a discontinuity forms in distribution of difference brightness or plasma density in the disturbed region front part. Since the u_C value is close to the local fast-mode MHD velocity, which in corona approximately equal to the Alfven one, the formation of such a discontinuity when u_C is exceeded may be identified with the formation of a shock wave.

[28] **Acknowledgments.** The SOHO/LASCO data used here are produced by a consortium of the Naval Research Laboratory (USA), Max-Planck-Institut fuer Aeronomie (Germany), Laboratoire d'Astronomie (France), and the University of Birmingham (UK). The CME catalog is

generated and maintained at the CDAW Data Center by NASA and The Catholic University of America in cooperation with the Naval Research Laboratory. SOHO is a project of international cooperation between ESA and NASA.

References

Billings, D. E. (1966), *A Guide to the Solar Corona*, Academic, New York.

Brueckner, G. E., et al. (1995), The large angle spectroscopic coronagraph (LASCO), *Sol. Phys.*, *162*, 357–402.

Ciaravella, A., J. C. Raymond, S. W. Kahler, A. Vourlidas, and J. Li (2005), Detection and diagnostics of a coronal shock wave driven by a partial-halo coronal mass ejection on 2000 June 28, *Astrophys. J.*, *621*, 1121–1128.

Cremades, H., and V. Bothmer (2004), On the three-dimensional configuration of coronal mass ejections, *Astron. Astrophys.*, *422*, 307–322.

Eselevich, M. V., and V. G. Eselevich (2007), First experimental studies a perturbed zone preceding the front of a coronal mass ejection, *Astron. Rep.*, *51*, 947–954.

Eselevich, M. V., and V. G. Eselevich (2008), About formation of a perturbed zone and a shock wave, excited by a coronal mass ejection, *Astron. Rep.*, in press.

Eselevich, M. V., V. G. Eselevich, and K. Fujiki (2007), Streamer belt and chains as the main sources of quasi-stationary slow solar wind, *Sol. Phys.*, *240*, 135–151.

Eselevich, V. G. (1995), New results on the site of initiation of coronal mass ejections, *Geophys. Res. Lett.*, *22*, 2681–2684.

Eselevich, V. G., V. G. Fainshtein, and G. V. Rudenko (1999), Study of the structure of streamer belts and chains in the solar corona, *Sol. Phys.*, *188*, 277–297.

Hundhausen, A. J. (1993), Sizes and locations of coronal mass ejections: SMM observations from 1980 and 1984–1989, *J. Geophys. Res.*, *98*, 13,177–13,200.

Jackson, B. V., and E. Hildner (1978), Forerunners: Outer rims of solar coronal transients, *Sol. Phys.*, *60*, 155–170.

Mancuso, S., J. C. Raymond, J. Kohl, Y.-K. Ko, M. Uzzo, and R. Wu (2002), UVCS/SOHO observations of a CME-driven shock: Consequences on ion heating mechanisms behind a coronal shock, *Astron. Astrophys.*, *383*, 267–274.

Mann, G., H. Aurass, A. Klassen, C. Estel, and B. J. Thompson (1999), Coronal transient waves and coronal shock waves, in *Plasma Dynamics and Diagnostics in the Solar Transition Region and Corona*, *Eur. Space Agency Spec. Publ.*, *ESA-SP 466*, 477.

Mouschovias, T. C., and A. I. Poland (1978), Expansion and broadening of coronal loop transients: A theoretical explanation, *Astrophys. J.*, *220*, 675–682.

Raymond, J. C., B. J. Thompson, O. C. St. Cyr, N. Gopalswamy, S. Kahler, M. Kaiser, A. Lara, A. Ciaravella, M. Romoli, and R. O'Neal (2000), SOHO and radio observations of a CME shock wave, *Geophys. Res. Lett.*, *27*, 1439–1442.

Wang, Y.-M., N. R. Sheeley Jr., D. G. Socker, R. A. Howard, and N. B. Rich (2000), The dynamical nature of coronal streamers, *J. Geophys. Res.*, *105*, 25,133–25,142.

M. V. Eselevich and V. G. Eselevich, Institute of Solar-Terrestrial Physics, Lermontova str. 126a, P.O. Box 291, Irkutsk 664033, Russia. (mesel@iszf.irk.ru; esel@iszf.irk.ru)